Transfer reactions in $^{32}S + ^{92,98,100}Mo$ and ^{93}Nb at near barrier energies

J. F. Liang, L. L. Lee, Jr., J. C. Mahon, and R. J. Vojtech*
Department of Physics, State University of New York at Stony Brook, Stony Brook, New York 11794
(Received 20 January 1994)

Differential cross sections for quasielastic transfer were measured for ^{32}S beams bombarding $^{92,98,100}Mo$ and ^{93}Nb targets at laboratory energies of 109, 116, and 125 MeV. Distorted-wave Born approximation calculations are in good agreement with the one-nucleon transfer data at all energies. Large transfer cross sections were observed for $^{98,100}Mo$ and ^{93}Nb targets which is consistent with the large sub-barrier fusion enhancement observed in the same systems. The transfer probability for one-nucleon transfer at large reaction distances is well described by the semiclassical model. There is a slope anomaly for two-proton stripping at energies just above the barrier but no anomaly for two-neutron pickup.

PACS number(s): 25.70.Hi

I. INTRODUCTION

Heavy ion collisions at energies in the vicinity of the Coulomb barrier involve considerable complexity. A number of reaction channels, such as fusion, nucleon transfer, and inelastic excitation can take place. The coupling among channels is important in determining the strength of an individual channel. For instance, some fusion excitation functions measured at energies below the barrier are orders of magnitude greater than predictions from the one-dimensional barrier penetration model [1,2]. This well known sub-barrier fusion enhancement can be explained by a channel coupling scheme [3,4]. Low-lying surface vibrational modes have been found to contribute appreciably to the enhancement [5]. In some cases, nucleon transfer [4,6,7] and/or higher excitations [8] have to be considered.

Fusion excitation functions for $^{32}S + ^{A}Mo$ and ^{93}Nb were measured by Pengo *et al.* [9] and Stelson *et al.* [10], respectively. For ^{92}Mo, the measurement is in good agreement with the barrier penetration model predictions. However, for the other molybdenum isotopes and ^{93}Nb, a significant enhancement in the cross sections was observed at energies below the barrier. In this work, we have measured nucleon transfer for $^{32}S + ^{92,98,100}Mo$ and ^{93}Nb at energies slightly above and below the barrier to make a qualitative comparison between the fusion and transfer.

A further goal of the experiments is to investigate the energy dependence of the transfer probability as a function of the distance of closest approach. For low energy heavy ion collisions, it is suitable to use the semiclassical approximation [11] in which transfer is described as nucleons tunneling through a potential barrier. At large reaction distances, where the nuclear absorption is negligible, the transfer probability falls exponentially as the distance increases [12]. The slope of the exponential falloff for two-nucleon transfer is expected to be approximately twice that for one-nucleon transfer. Many experimental results showed good agreement between theory and experiment [13]. However, it was observed in some experiments that the slope for two-nucleon transfer is smaller than predicted [14–17]. Often, it is similar to the slope for one-nucleon transfer. This is referred to as the "slope anomaly." Rehm *et al.* [18] studied the systematics of two-neutron transfer at large distances and showed that the slope anomaly should disappear as energies approached the barrier from above. Furthermore, the slope anomaly at higher energies can be attributed to the influence of diffractive scattering since two-nucleon transfer has a more localized form factor.

The experimental methods and data reduction are described in the following section. The angular distributions of one- and two-nucleon transfer and the comparison with distorted-wave Born approximation (DWBA) predictions are presented in Sec. III, while in Sec. IV, the transfer excitation functions are qualitatively compared with the fusion yields. In Sec. V, the one- and two-nucleon transfer at large reaction distances is discussed and compared with the semiclassical model. The conclusions are given in Sec. VI.

II. EXPERIMENTS AND DATA

^{32}S beams of energies of 109, 116, and 125 MeV were obtained from the tandem-linac accelerator at the Stony Brook Nuclear Structure Laboratory. The targets are isotopically enriched self-supporting foils of thickness 310, 490, 290, and 170 $\mu g/cm^2$ for $^{92,98,100}Mo$ and ^{93}Nb, respectively.

The experimental setup is shown in Fig. 1. Six surface barrier Si detectors (SBD's) and four E-ΔE Si gas telescopes, mounted on two movable tables, were used to detect projectilelike reaction products. The angular interval between detectors was 10°. The charge of the

*Present address: EG & G Energy Measurements, Washington Aerial Measurements Department, Suitland, MD 20764.

 ©1994 The American Physical Society

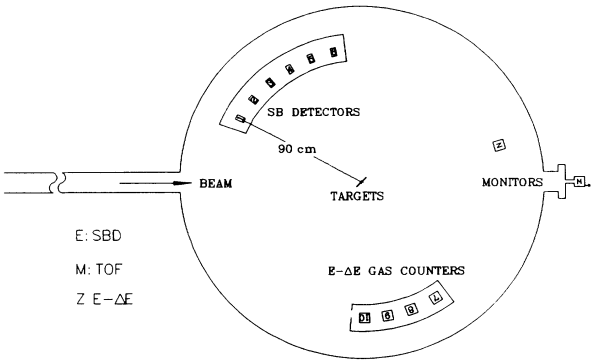

FIG. 1. Apparatus for transfer products identification.

transfer product was identified by the gas telescopes. The E-ΔE telescopes were filled with P10 gas at pressures such that particles lost 1/4 to 1/2 of their energies in the gas. Since the energies of the transfer products are too low for charge identifications at backward angles, the gas telescopes could only be used at forward angles. For comparison purposes, one or two surface barrier detectors were placed at angles which overlapped with the gas telescopes.

Mass identification was achieved by measuring the energy and time of flight of the particles. A 90 cm flight path was provided by the scattering chamber. Time pick-off units were placed behind each Si detector to obtain the fast timing signal. The detector triggers were used as start pulses for a time to pulse height convertor and the linac rf signals were used as common stop pulses; ten detectors were used simultaneously. The timing width of the beam was determined by measuring the elastic scattering from a 100 $\mu g/cm^2$ Au foil. During the experiment, the full width at half maximum (FWHM) of the beam was between 150 and 200 ps.

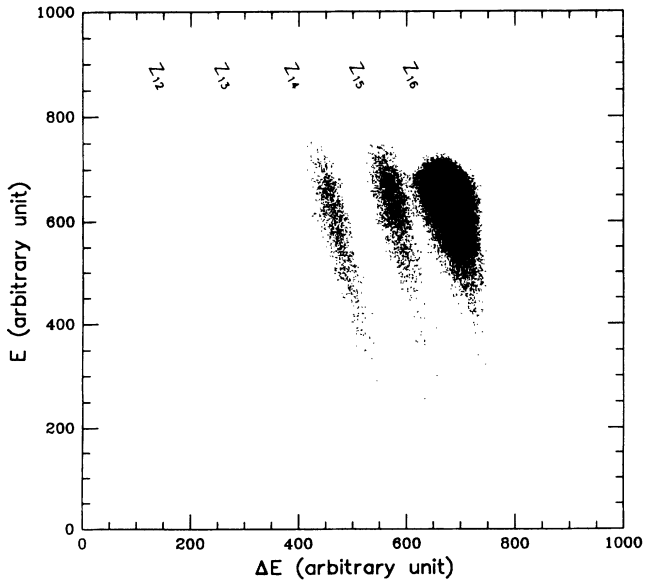

FIG. 2. 2D histogram of E vs ΔE for 125 MeV $^{32}S + ^{100}Mo$ at $\theta_{lab} = 80°$.

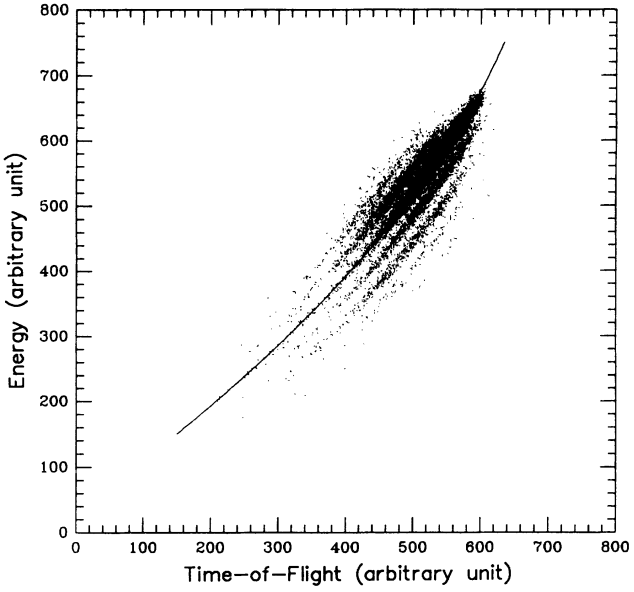

FIG. 3. 2D histogram of E vs TOF for 125 MeV $^{32}S + ^{100}Mo$ at $\theta_{lab} = 90°$. The solid curve is a parabola fitted to the elastic scattering data for linearization.

An example of energy versus energy loss two-dimensional histogram from a E-ΔE telescope is presented in Fig. 2. Only charge stripping was observed. The energy versus time-of-flight (TOF) two-dimensional (2D) histogram from a SBD is shown in Fig. 3. The mass spectrum, as shown in Fig. 4, was obtained by linearizing the 2D histogram and projecting on the TOF axis. Up to three-nucleon pickup and four-nucleon stripping were observed. By comparison with the charge gated mass spectrum from the E-ΔE telescopes, shown in Fig. 5, it is observed that the pickup is primarily neutron pickup and the stripping is dominated by proton stripping, consistent

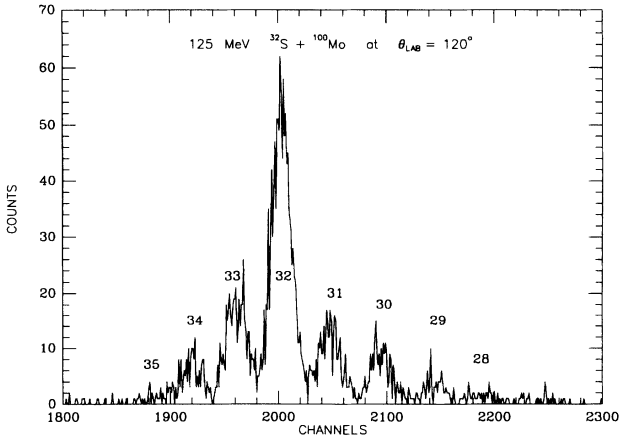

FIG. 4. Mass spectrum obtained by linearizing the E-TOF 2D histogram and projecting on the TOF axis. Shown here is an example of 125 MeV $^{32}S + ^{100}Mo$ at $\theta_{lab} = 120°$.

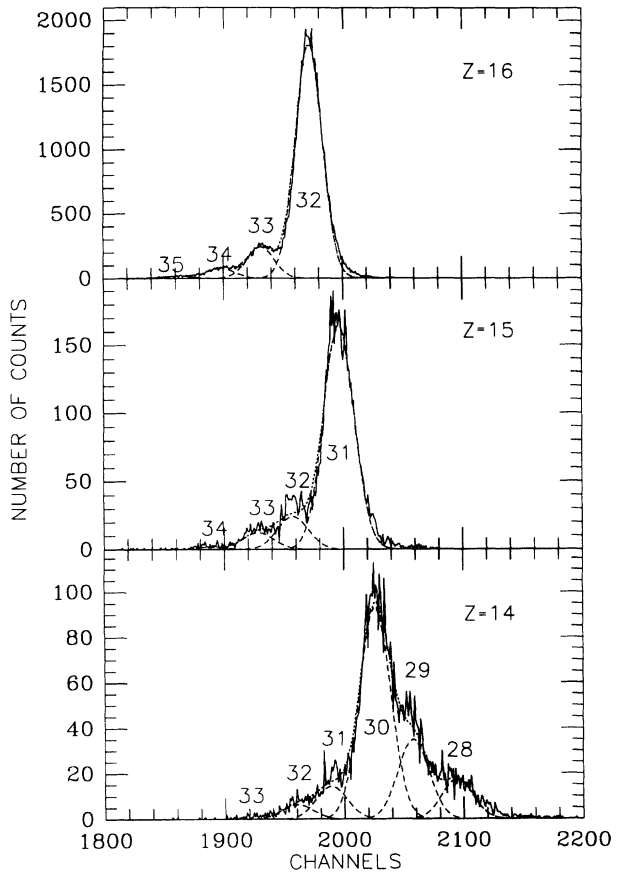

FIG. 5. Charge gated mass spectra from a E-ΔE telescope at $\theta_{\rm lab} = 80°$ for 125 MeV ^{32}S + ^{100}Mo. The areas of the mass peaks were extracted by fitting the spectra with Gaussian distributions which are shown by the dashed curves. The dotted curves are the summed total of the fit.

with Q-value expectations. The major transfer channels identified are $+2n, +1n, -1p, -2p, -2p1n(-^3\mathrm{He})$, and $-2p2n(-\alpha)$. In the E-ΔE telescopes, the yields of the other channels, such as $-1p + 2n$ and $-2p + 1n$, are less than 10% of the $+1n$ and $-1p$ channels, respectively. At the energy of 109 MeV, the yields of the weaker channels are too small to be significant.

The energy resolution of this experiment was between 3 and 4 MeV. It was limited by the energy spread of the beam. Additionally, at the backward angles, the target thickness was a major factor because of the reflection geometry. An example of the energy distributions of the transfer products is shown in Fig. 6 for two-proton stripping. The centroid of the energy spectrum is located around the optimum Q value ($Q_{\rm opt}$) [19] which is derived from smoothly matching the trajectories before and after the transfer. The optimum Q value is given by

$$Q_{\rm opt} = \left(\frac{Z_p' Z_t'}{Z_p Z_t} - 1\right) E_{\rm c.m.}, \qquad (1)$$

where Z_p and Z_t are the atomic number of the projectile and target, respectively, Z_p' and Z_t' the atomic number of the ejectile and recoil respectively, and $E_{\rm c.m.}$ the center of mass energy. This is the evidence that the reaction

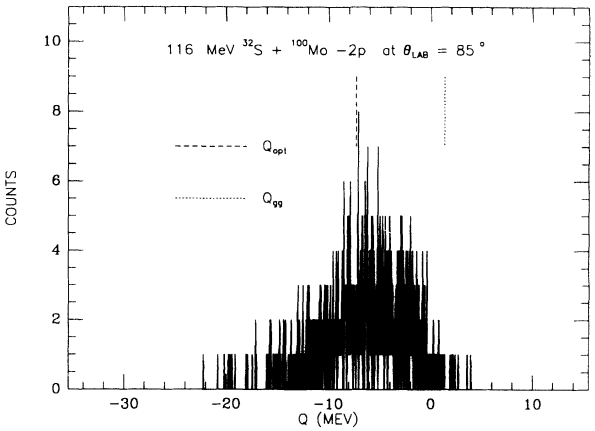

FIG. 6. Energy spectrum of 116 MeV ^{32}S + ^{100}Mo at $\theta_{\rm lab} = 85°$.

follows the Coulomb trajectory. Therefore, the semiclassical model should be applicable.

III. ANGULAR DISTRIBUTIONS

The elastic scattering and transfer cross sections were obtained by normalizing data to the most forward angle detector where the elastic scattering events were assumed to be the same as the Rutherford scattering. Due to the finite energy resolution, the elastic scattering events could not be separated from the inelastic scattering. Moreover, only energy-integrated transfer cross sections were obtained. The ratio of the "elastic" (plus inelastic) to Rutherford scattering as a function of angle is shown in Fig. 7. The curves shown in the figure are results of optical model calculations fitting to the data. The optical potential parameters obtained from the fits are listed in Table I. For the 125 MeV data, the disagreement between the data and calculations at large scattering angles is probably caused by the contribution from inelastic scattering events.

The one- and two-nucleon transfer angular distributions were compared to predictions of distorted-wave Born approximation (DWBA) calculations using the computer code PTOLEMY [20]. The one-nucleon transfer calculations included states of excitation energies up to 3.0 MeV for both projectile and target. The DWBA cross section is given by

$$\sigma = \sum_{p,t} S_p S_t \sigma_{pt}, \qquad (2)$$

where S_p and S_t refer to the spectroscopic factors of the projectile and target, respectively, and σ_{pt} is the calculated cross section of the corresponding state. The spectroscopic factors were obtained from light ion experiments. The optical potential parameters in the DWBA calculations were obtained from the elastic scattering analysis.

Figure 8 presents the one-proton stripping angular distributions for the ^{98}Mo target. As expected, the peak of the angular distribution shifts toward 180° as the energy

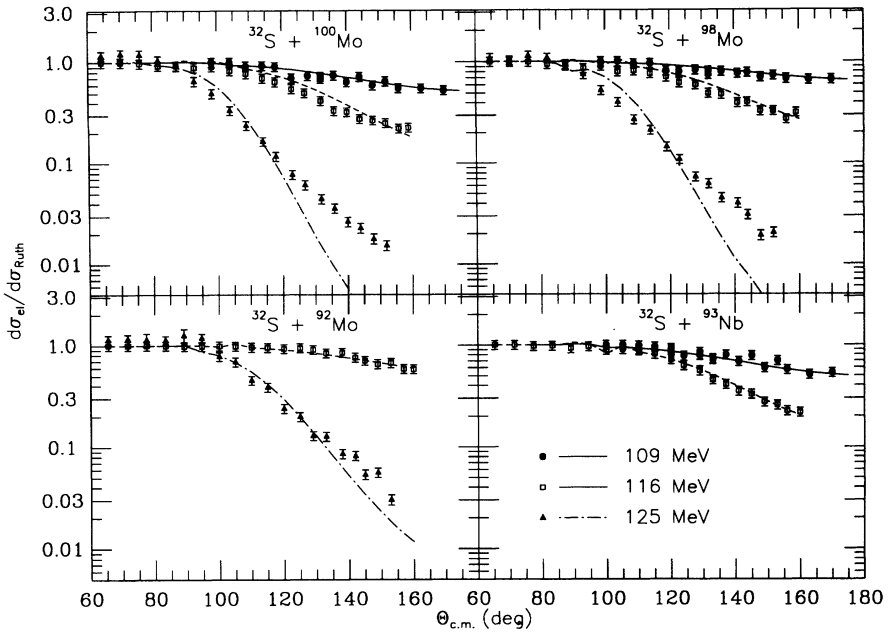

FIG. 7. The ratio of the elastic to Rutherford scattering cross section as a function of the center-of-mass angle. The curves are results of the optical model calculation.

decreases. The curves correspond to results of DWBA calculations. For $^{98,100}Mo$ targets, the predictions of DWBA calculations were multiplied by factors between 1.4 and 2.0 to normalize the calculations to the data. For all the other targets and all the one-neutron transfer data, no normalization is necessary. For all the targets, the 125 MeV data peak forward by 10°–12.5° compared with the DWBA calculations. The curves were shifted forward in the figure to compare with the data. This forward shift in the angular distribution has been observed in some other systems [16,21,22]; it may be due to multistep processes involved in the transfer reaction. The DWBA calculations also underpredict the 125 MeV data at backward angles. This is probably due to a large overlap of the reaction nuclei where different reaction mechanisms may take place. Very good agreement between the data and the calculations is shown at energies of 116 and 109 MeV, particularly at small angles. The angular distributions for one-neutron pickup are similar to the case for one-proton stripping. No normalization factor is required to scale the DWBA calculations to the data for all the targets.

The calculations for the 116 MeV reactions overpredict the measured cross sections at the far backward angles. The difference is more significant for neutron pickup than for proton stripping. If only the ground state to ground state transfer calculation is performed and ar-

TABLE I. Optical model potential parameters obtained from the elastic scattering data. V is the depth for the real potential, r_0 the radius parameter, a the diffuseness parameter, and r_{C0} the Coulomb radius parameter.

V (MeV)	$r_0 = r_{I0}$ (fm)	$a = a_I$ (fm)	r_{C0} (fm)
67.58	1.10	0.69	1.32

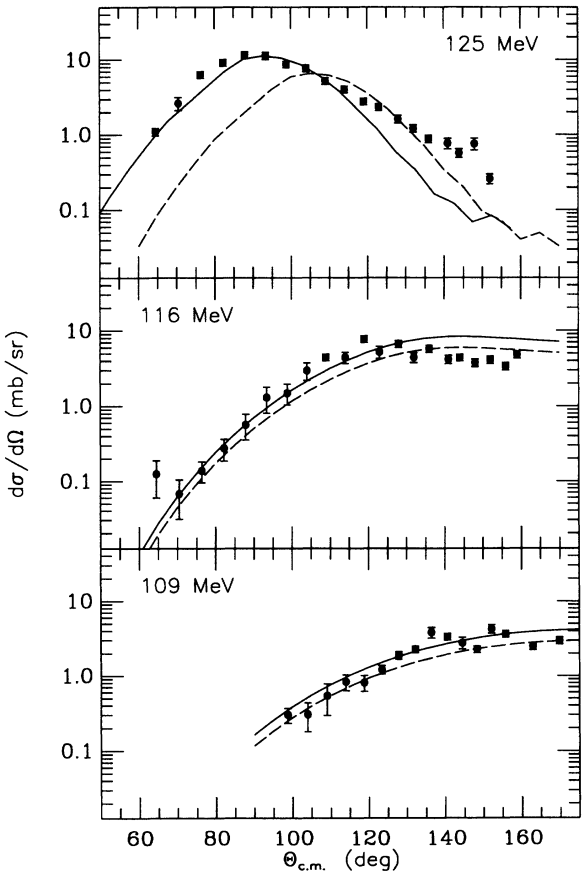

FIG. 8. Angular distributions for the ^{32}S + ^{98}Mo one-proton stripping. The dashed curves are results of DWBA calculations described in the text. The calculations, normalized to the data, are shown by the solid curves.

bitrarily normalized to the data, a better agreement in the shape of the angular distributions is reached for proton stripping as shown in Fig. 9. Including more excited states in the calculation makes no significant change at the forward angles. However, the deviation gets larger at the backward angles as more excited states are included in the calculation. For neutron pickup calculations, a small difference is seen at the backward angles even for the ground state to ground state transfer calculations. This is also shown in Fig. 9. When more excited states are included, the deviation becomes larger. Glendenning and Wolschin [23] have shown that indirect processes can interfere with the direct processes destructively and the cross sections will be smaller than those calculated by DWBA which models direct processes only.

Two-proton stripping angular distributions for the ^{98}Mo target are shown in Fig. 10. The DWBA calculation was carried out by assuming a cluster transfer mechanism [24]. Only ground state to ground state transfer was calculated. The curves shown in the figure are results of the calculations arbitrarily normalized to the data. The 125 MeV data also peak forward as compared to the calculations. The curve shown is a forward shifted result. As in the case of one-nucleon transfer, there is enhancement in the backward angles for the 125 MeV data. The 116 MeV data disagree with the calculations at forward angles. This will be discussed in Sec. V.

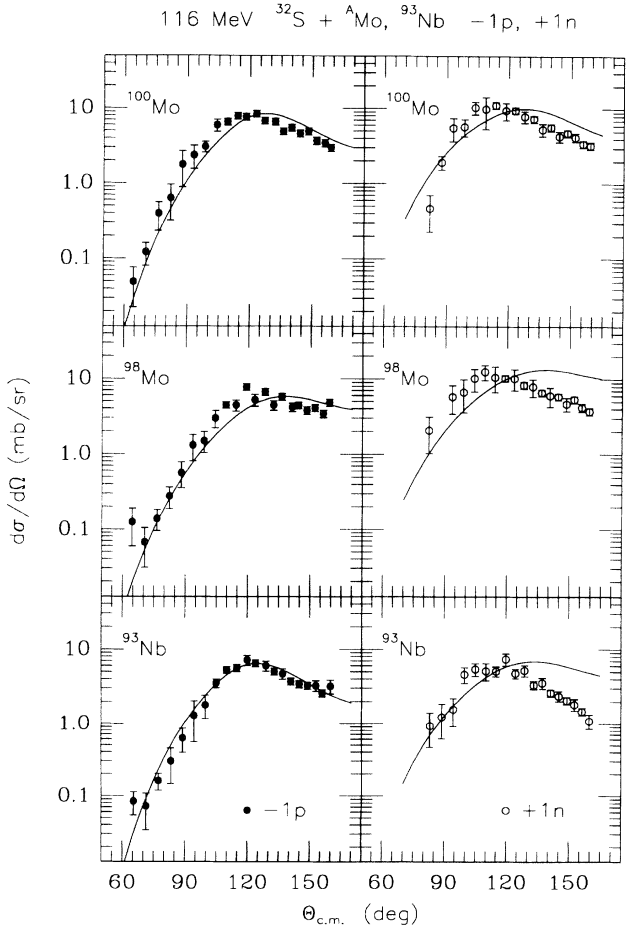

FIG. 9. The ground state to ground state transfer DWBA calculations compared to the one-proton stripping and one-neutron pickup data. The curves are arbitrarily normalized to the data.

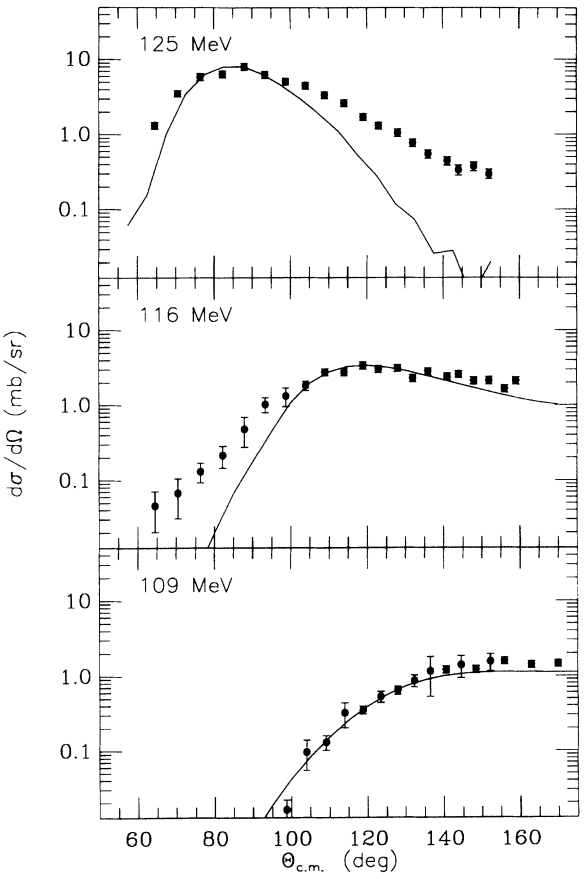

FIG. 10. Angular distributions for the ^{32}S + ^{98}Mo two-proton stripping. The solid curves are results of DWBA calculations described in the text normalized to the data.

IV. CORRELATION OF TRANSFER AND FUSION

The transfer total cross section was obtained by integrating the angular distributions over angles. Table II lists the energy- and angle-integrated few-nucleon transfer cross sections; the uncertainties are shown in the parentheses. The cross section for one-neutron pickup is comparable to or slightly larger than that for one-proton stripping. The yields for one-nucleon transfer are 2–3 times greater than for two-nucleon transfer. For ^{98,100}Mo, the three-nucleon transfer cross section is larger than the four-nucleon transfer by factors of 2–3. For ^{92}Mo the four-nucleon transfer cross sections are greater than the three-nucleon transfer and are slightly larger than the two-proton stripping. This is due to the Q-value considerations which favor four-nucleon stripping in that

TABLE II. Energy- and angle-integrated transfer cross sections (in mb).

E_{lab} (MeV)	$-2p,-2n$	$-2p,-1n$	$-2p$	$-1p$	$+1n$	$+2n$
	^{100}Mo					
125	3.9 (0.9)	9.3 (1.5)	36 (4)	56 (6)	73 (20)	40 (14)
116	1.6 (0.3)	3.5 (0.5)	18 (2)	34 (5)	45 (10)	13 (2)
109	0.3 (0.1)	0.84 (0.25)	6.3 (0.9)	14 (2)		
	^{98}Mo					
125	4.3 (0.7)	9.3 (1.1)	30 (3)	44 (5)	66 (14)	26 (8)
116	1.3 (0.3)	2.5 (0.4)	14 (2)	25 (4)	49 (13)	13 (2)
109	0.16 (0.06)	0.4 (0.2)	3.6 (0.8)	9.1 (1.4)		
	^{92}Mo					
125	18.3 (2.0)	10.2 (1.2)	11.0 (1.9)	20 (3)	34 (13)	15 (6)
116	3.1 (0.5)	1.1 (0.3)	2.8 (0.8)	11 (2)		
	^{93}Nb					
116	4.0 (0.6)	3.9 (0.6)	12 (2)	25 (4)	25 (5)	7.9 (1.9)
109	0.54 (0.15)	0.58 (0.16)	3.9 (0.7)	10 (2)		

case. For ^{93}Nb, the yields for three- and four-nucleon stripping are comparable. The multinucleon (two to four) transfer cross sections are about 30–40 % of the total transfer cross sections for all targets.

Note that the yields of neutron transfer for ^{92}Mo at 116 MeV were too small to be measured. For the energy of 109 MeV, the neutron transfer data were contaminated by the tail of the elastic scattering for all targets. It is difficult to extract them without having large uncertainties. Therefore, they are not listed in the table.

The total transfer cross sections were obtained by summing the cross sections over all the channels in Table II. In Table III, the total transfer cross sections and the fusion cross sections [9,10] are compared with the total reaction cross sections which were calculated by the optical model. The sum of the transfer and the fusion cross section make up the total reaction cross section, since the optical potential parameters were obtained from fitting the elastic plus the inelastic scattering data. The total transfer cross sections are 30–40 % of the total reaction cross sections. For molybdenum isotopes, the cross sections increase as the number of neutrons in the isotope increases.

The fusion excitation functions measured by Pengo *et al.* [9] for ^{A}Mo and by Stelson *et al.* [10] for Nb are shown in Fig. 11. The solid curves through the data points are used for guiding the eyes. The dotted curves are the results of one-dimensional barrier penetration calculations [25]. Disagreement between the fusion data and the calculations can be seen, particularly at energies well below the barrier. Coupled-channel calculations, using the code CCFUS [26], were performed by including the first 2^+ and 3^- states of S and Mo. The results are shown by the dashed curves. As can be seen, the results of the coupled-channel calculations agree with the data only for the ^{92}Mo target. For the other targets, coupling the inelastic channels cannot fully account for the sub-barrier fusion enhancement. In this case, coupling the transfer channels should be considered for the $^{98,100}Mo$ and ^{93}Nb targets. The one- and two-nucleon transfer cross sections measured in this work are shown in Fig. 12; the fusion excitation functions are shown for comparison. The results of one- and two-neutron pickup at energies well below the barrier [27] are also included in this figure. The transfer cross sections fall less steeply than the fusion cross sections as the energies go down. At energies $\approx 10\%$ below the barrier, transfer reactions become the dominant reaction channels. The transfer excitation function for ^{92}Mo shows steeper falloff than all the other targets.

Although the neutron transfer for $^{98,100}Mo$ and ^{93}Nb has positive Q values, particularly for two-neutron pickup, the yields for proton transfer are not much less than the neutron transfer. It has been pointed out [28,29] that charge transfer with a negative Q value could also enhance fusion if the Q-matching conditions for transfer are valid. Furthermore, coupled-channel calculations show that multinucleon transfer plays an important role in the fusion enhancement [30]. The sub-barrier fusion enhancement would depend on the average behavior of the transfer rather than by the Q value of specific channels. By comparing with Table III, the correlation between transfer and fusion can be seen. Small transfer cross sections were observed for the ^{92}Mo target where there is little fusion enhancement; large transfer cross sec-

TABLE III. Total transfer, fusion, and total reaction cross sections (in mb) for $^{32}S + {}^{A}Mo$ and ^{93}Nb.

E_{lab} (MeV)	σ (mb)	^{92}Mo	^{98}Mo	^{100}Mo	^{93}Nb
125	σ_{tr}	107 (28)	178 (31)	220 (46)	
	σ_{fu}	> 254	> 347	> 300	
	σ_R	396	481	556	
116	σ_{tr}	27 (3)	104 (22)	116 (20)	77 (14)
	σ_{fu}	50	116	141	155
	σ_R	85	181	213	215
109	σ_{tr}		13 (2)	22 (3)	15 (3)
	σ_{fu}		36	38	37

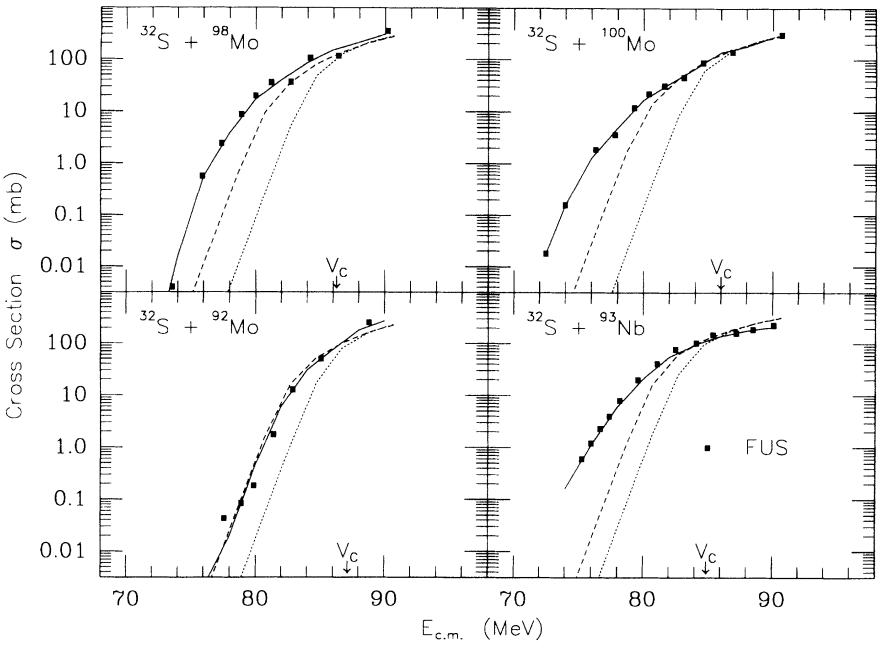

FIG. 11. Fusion excitation functions for ^{32}S + ^{A}Mo and ^{93}Nb. The solid curves through the data are to guide the eyes. The dotted curve are results of one-dimensional barrier penetration calculations. The dashed curves are results of coupled-channel calculations coupling the first 2^+ and 3^- states of S and Mo inelastic channels. The experimental points are from Refs. [9,10].

tions were observed for ^{98,100}Mo and ^{93}Nb targets where there is large sub-barrier fusion enhancement.

V. TRANSFER PROBABILITY

At reaction energies near the Coulomb barrier, nucleon transfer between heavy ions is often described by the semiclassical model; the projectile is assumed to follow the classical Coulomb trajectory [12] and the nucleon transfer takes place at the distance of closest approach. The transfer mechanism can be treated as nucleons tunneling through a potential barrier [31].

The transfer probability is introduced to describe nucleon transfer at large reaction distances. It is defined as the ratio of the transfer cross sections measured at angle Θ to the incident flux and is given by [32]

$$P_{\rm tr} = \frac{d\sigma_{\rm tr}}{|2\pi b db|}, \tag{3}$$

where b is the impact parameter corresponding to the scattering angle Θ. By expressing the impact parameter b explicitly in terms of the reaction parameters, the transfer probability can be written as

$$P_{\rm tr} = \frac{d\sigma_{\rm tr}/d\Omega}{d\sigma_{\rm Ruth}/d\Omega}, \tag{4}$$

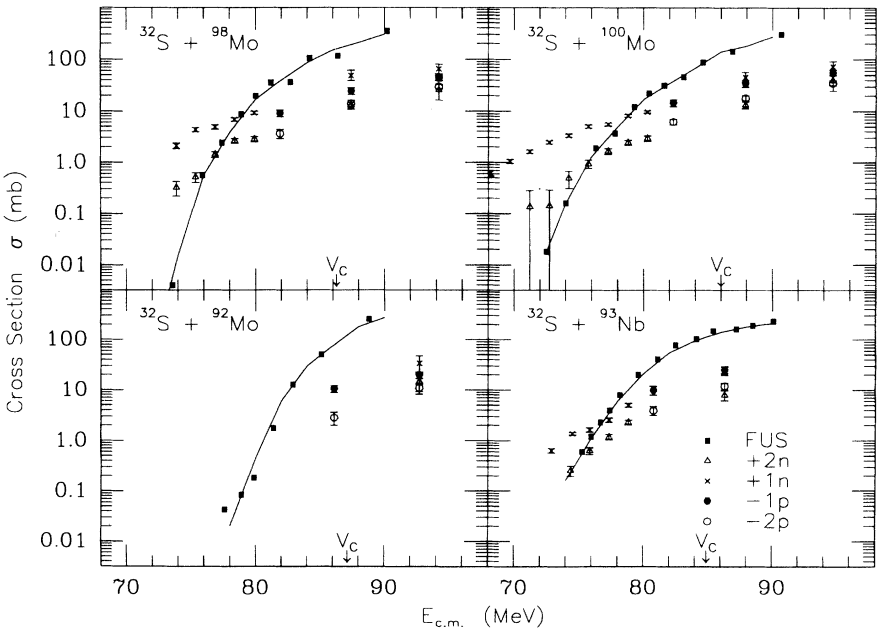

FIG. 12. One- and two-nucleon transfer cross sections as a function of energy for ^{32}S + ^{A}Mo and ^{93}Nb. The solid squares are the fusion excitation functions from Refs. [9,10]. The solid curves through the data are to guide the eyes.

where $d\sigma_{\rm Ruth}/d\Omega$ is the the corresponding Rutherford cross section. Equation (4) was used to extract the transfer probability from the data.

At large reaction distances where the overlap between two nuclei is insignificant, the transfer probability is given by the semiclassical approximation as [12]

$$P_{\rm tr} \propto \sin\left(\frac{\Theta}{2}\right) \exp(-2\alpha D), \tag{5}$$

where D is the distance of closest approach which is normally calculated from the Coulomb trajectory and the slope parameter $\alpha = \sqrt{2\mu E_b}/\hbar$; μ is the reduced mass and E_b is the binding energy of the transferred nucleon. If the transfer probability is plotted as a function of D, it falls exponentially with a slope 2α at large distances. Note that for two-nucleon transfer, the slope is expected to be twice that for one-nucleon transfer for both sequential and simultaneous transfer.

The influence of the nuclear absorption should be excluded when the transfer probability is compared with the semiclassical model. In Fig. 13, the ratio of the elastic to Rutherford scattering cross section is plotted as a function of the overlap parameter $d_0 = D/(A_p^{1/3} + A_t^{1/3})$. Here, A_p and A_t are the mass of the projectile and target, respectively. As can be seen from the figure, the ratio becomes less than 1 at $d_0 < 1.6$ fm for all the targets at all energies. This suggests that the nuclear absorption becomes negligible at $d_0 \geq 1.6$ fm. Therefore, only data at $d_0 \geq 1.6$ fm will be considered here.

The transfer probability for one- and two-proton stripping is plotted as a function of the overlap parameter in Fig. 14. The lines are results from DWBA calculations which are compared to the data at $d_0 \geq 1.6$ fm since the DWBA is equivalent to the semiclassical model at these energies. All the one-proton stripping data agree with the DWBA calculations. For two-proton stripping, the data agree with the DWBA calculations only at energies below the Coulomb barrier. At energies above the barrier, the two-proton stripping data have slopes similar to those for one-proton stripping but disagree with DWBA calculations which predict greater slopes. There is a slope anomaly for two proton stripping at energies above the barrier but no anomaly at energies below the barrier. The slope behavior changes sharply right at the barrier for two-proton stripping.

Figure 15 presents the transfer probability for neutron pickup at the laboratory energy of 116 MeV which is 1%–2% above the barrier. As can be seen, the data and DWBA predictions, shown by solid lines, are in good agreement for both one- and two-neutron pickup; the slope for two-neutron transfer is greater than that for one-neutron transfer as expected from the semiclassical model. This agrees with the systematics for neutron transfer [18] which expect no slope anomaly for two-neutron transfer at energies in the vicinity of the Coulomb barrier.

As suggested in the articles by Wuosmaa *et al.* [17], Liang *et al.* [33], and Rehm *et al.* [18], the energy dependence of the slope anomaly for two-nucleon transfer restricts the applicability of the semiclassical model. The width of the partial wave distribution Δl can be used to determine whether the semiclassical model is valid. The transfer cross section expressed in the partial wave expansion is given by

$$\frac{d\sigma}{d\Omega} = \left| \frac{1}{2ik} \sum_l (2l+1)\eta_l \exp(2i\sigma_l) P_l(\cos\Theta) \right|^2, \tag{6}$$

where σ_l is the Coulomb phase shift, η_l a parametrized form factor, and P_l the Legendre polynomials. The width Δl of the partial wave distribution is associated with the width of the form factor η_l. It is suitable to use the

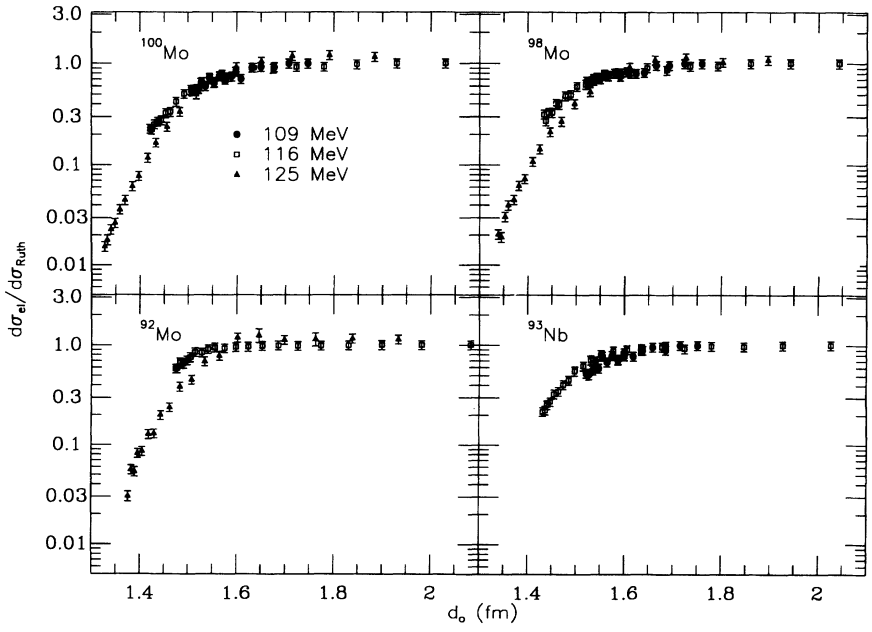

FIG. 13. The ratio of the elastic to the corresponding Rutherford scattering cross section as a function of the overlap parameter d_0.

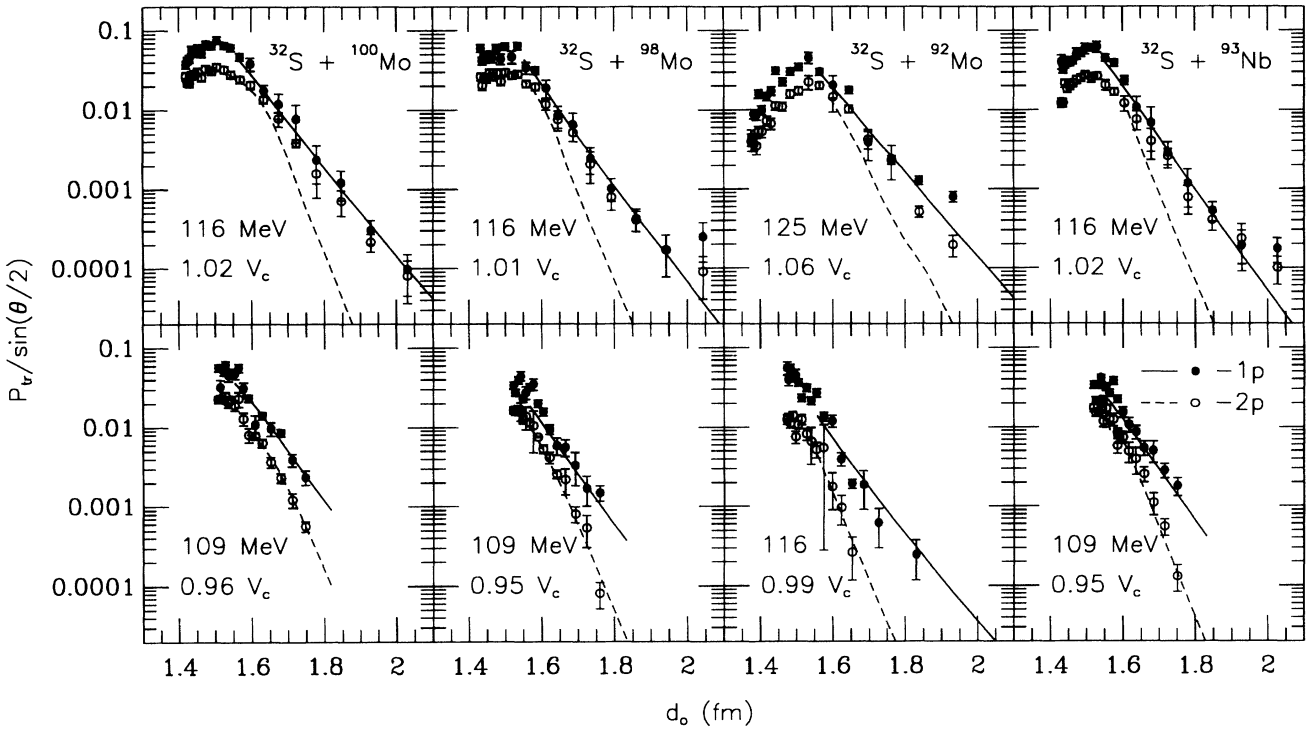

FIG. 14. The transfer probability of one- and two-proton stripping as a function of d_0.

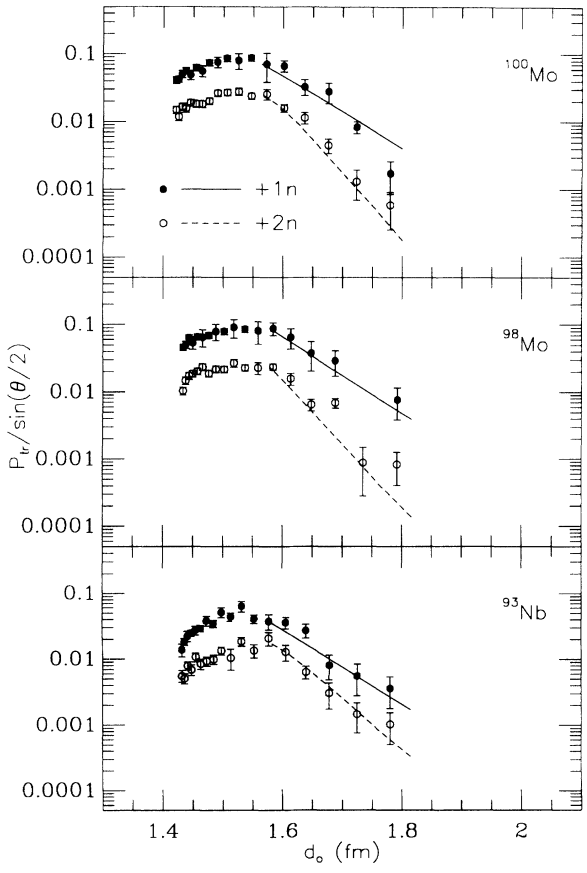

FIG. 15. The transfer probability of one- and two-neutron pickup as a function of d_0 at the energy of 116 MeV.

semiclassical model when Δl is greater than a critical width [17,18]

$$\Delta l_c = \frac{\sqrt{n}}{\sin(\Theta_0/2)}, \tag{7}$$

where n is the Sommerfeld parameter and Θ_0 is the angle corresponding to the maximum of the angular distribution. When the reaction is very localized in l space, $\Delta l < \Delta l_c$, it becomes a quantal diffraction process.

The partial wave expansions of one- and two-proton stripping were performed to investigate the dominant reaction mechanism. The form factor η_l was obtained from the S matrix in the DWBA calculation at 125 MeV. The shape of the η_l was not adjusted for the 116 and 109 MeV calculations. Only the centroid of the η_l was shifted to the corresponding grazing angular momentum. The width of the η_l is of the order of $20\hbar$ for both one- and two-proton transfer while the critical value Δl_c varies from $7\hbar$ to $8\hbar$ depending on the reaction system and energy. This suggests that the reaction can be described by the semiclassical model which is consistent with the equivalence of DWBA and the semiclassical model at these energies.

As shown previously [33], these partial wave calculations for one-proton stripping not only reproduce the results of DWBA calculation but also are in good agreement with the data. Moreover, the partial wave expansions for two-proton stripping are consistent with the data at energies below the barrier. However, at energies above the barrier, the calculations underpredict the data at small scattering angles, which correspond to large distances of closest approach as shown in Fig. 16.

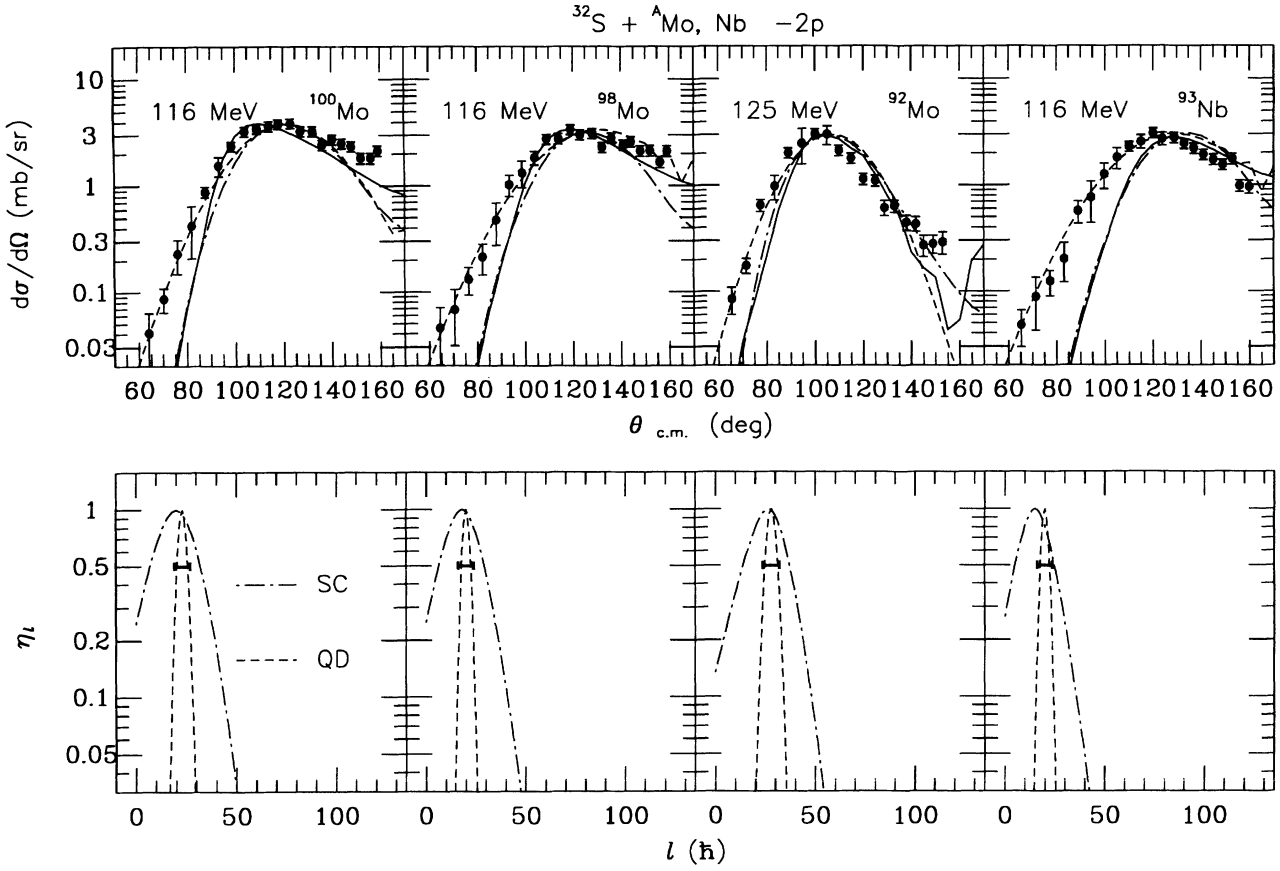

FIG. 16. Angular distributions for two-proton stripping. The solid curves are results of DWBA calculations. The dashed and dash-dotted curves are results of partial wave calculations using form factors shown in the bottom panel. The solid bars indicate the critical width for Δl.

This suggests that a different reaction process, besides the semiclassical tunneling, is involved. As shown in Fig. 16, calculations using narrow form factors reproduce the two-proton stripping angular distributions. In particular, they agree with the data very well at forward angles. The width of the form factors $\Delta l \simeq 5\hbar$, which is smaller than the critical value shown by solid bars. Normally two-nucleon transfer has a narrower form factor, or l distribution, than one-nucleon transfer does. If the transfer mechanism involves multistep processes, the form factor could be much more localized [34]. The localization in l space would lead to a diffraction process. For this reason, the slope anomaly for two-proton stripping may be influenced by diffractive scattering.

VI. SUMMARY AND CONCLUSIONS

To summarize, the identified transfer channels are consistent with the expectations from Q-matching conditions. The measured one- and two-nucleon transfer angular distributions are in reasonably good general agreement with DWBA predictions. Large transfer cross sections were observed for ^{98,100}Mo and ^{93}Nb while small transfer cross sections were observed for ^{92}Mo. This is consistent with the large sub-barrier fusion enhancement observed in ^{98,100}Mo and ^{93}Nb, but not in ^{92}Mo.

The transfer probability for both one-proton and one-neutron transfer at large reaction distances, $d_0 \geq 1.6$ fm, is well described by the semiclassical model. For two-proton transfer, an anomalous slope behavior was observed at energies just above the Coulomb barrier. The slope anomaly disappears at energies below the barrier. For two-neutron transfer, there is no slope anomaly observed at any energies studied here which agrees with the systematics of two-neutron transfer. The partial wave expansions studied suggest that the slope anomaly is probably due to a very narrow form factor which may lead to diffractive scattering.

At this point, it is not understood why the slope behavior for two-proton transfer changes sharply right at the barrier. Additionally, it is not clear why there is a slope anomaly for two-proton stripping but no anomaly for two-neutron pickup at energies slightly above the bar-

rier. Is there difference in the mechanism of transferring protons and neutrons? Or is the mechanism of neutron pickup different from proton stripping? More measurements, particularly of proton transfer, will be needed to determine whether these are isolated cases or a systematic trend.

ACKNOWLEDGMENTS

One of us (J.F.L.) wishes to thank R. Vandenbosch for critically reading this manuscript and for helpful discussions. This work was supported by the National Science Foundation.

[1] M. Beckerman, Phys. Rep. **129**, 145 (1985).
[2] M. Beckerman, Rep. Prog. Phys. **51**, 1047 (1988).
[3] C. H. Dasso, S. Landowne, and A. Winther, Nucl. Phys. **A405**, 381 (1983).
[4] C. H. Dasso, S. Landowne, and A. Winther, Nucl. Phys. **A407**, 221 (1983).
[5] S. Landowne and S. C. Pieper, Phys. Rev. C **29**, 1352 (1984).
[6] R. A. Broglia, C. H. Dasso, S. Landowne, and G. Pollarolo, Phys. Lett. **133B**, 34 (1983).
[7] *Heavy Ion Interactions around the Coulomb Barrier*, Legnaro, Italy, 1988, edited by C. Signorini, S. Skorka, P. Spalaore, and A. Vitturi, Lecture Notes in Physics, Vol. 317 (Springer-Verlag, Berlin, 1988).
[8] H. Esbensen and S. Landowne, Phys. Rev. C **35**, 2090 (1987).
[9] R. Pengo, D. Evers, K. E. G. Löbner, U. Quade, K. Rudolph, S. J. Skorka, and I. Weidl, Nucl. Phys. **A411**, 255 (1983).
[10] P. H. Stelson, H. J. Kim, M. Beckerman, D. Shapira, and R. L. Robinson, Phys. Rev. C **41**, 1584 (1990).
[11] G. Breit, *Encyclopedia of Physics* (Springer, Berlin, 1959), Vol. 41.
[12] R. Bass, *Nuclear Reactions with Heavy Ions* (Springer-Verlag, Berlin, 1980).
[13] C. Y. Wu, W. von Oertzen, D. Cline, and M. W. Guidry, Annu. Rev. Nucl. Part. Sci. **40**, 285 (1990), and references therein.
[14] C. Y. Wu *et al.*, Phys. Lett. B **188**, 25 (1987).
[15] S. Juutinen *et al.*, Phys. Lett. B **192**, 307 (1987).
[16] W. von Oertzen, H. G. Bohlen, B. Gebauer, R. Künkel, F. Pühlhofer, and D. Schüll, Z. Phys. A **326**, 463 (1987).
[17] A. H. Wuosmaa, K. E. Rehm, B. G. Glagola, Th. Happ, W. Kutschera, and F. L. H. Wolfs, Phys. Lett. B **255**, 316 (1991).
[18] K. E. Rehm, B. G. Glagola, W. Kutschera, F. L. H. Wolfs, and A. H. Wuosmaa, Phys. Rev. C **47**, 2731 (1993).
[19] P. J. A. Buttle and L. J. B. Goldfarb, Nucl. Phys. **A176**, 299 (1971).
[20] M. H. Macfarlane and S. C. Pieper, Report No. ANL-76-11 Rev. 1, 1978 (unpublished).
[21] D. G. Kovar, B. G. Harvey, F. D. Becchetti, J. Mahoney, D. L. Hendrie, H. Homeyer, W. von Oertzen, and M. A. Nagarajan, Phys. Rev. Lett. **30**, 1075 (1973).
[22] F. L. H. Wolfs, K. E. Rehm, W. C. Ma, J. P. Schiffer, and T. F. Wang, Phys. Rev. C **45**, 2283 (1992).
[23] N. K. Glendenning and G. Wolschin, Nucl. Phys. **A281**, 486 (1977).
[24] W. D. Mayer, D. Pereira, K. E. Rehm, H. J. Scheerer, H. J. Körner, G. Korschinek, W. Mayer, P. Sperr, S. C. Pieper, and R. D. Lawson, Phys. Rev. C **26**, 500 (1982).
[25] D. L. Hill and J. A. Wheeler, Phys. Rev. **89**, 1102 (1953).
[26] C. H. Dasso and S. Landowne, Comput. Phys. Commun. **46**, 187 (1987).
[27] R. B. Roberts, S. B. Gazes, J. E. Mason, M. Satteson, S. G. Teichmann, L. L. Lee, Jr., J. F. Liang, J. C. Mahon, and R. J. Vojtech, Phys. Rev. C **47**, R1831 (1993).
[28] K. M. Hartmann and D. H. E. Gross, Z. Phys. A **311**, 131 (1983).
[29] W. Henning, F. L. H. Wolfs, J. P. Schiffer, and K. E. Rehm, Phys. Rev. Lett. **58**, 318 (1987).
[30] T. Winkelmann *et al.*, in *Proceedings of the Workshop Heavy Ion Collisions at Energies Near the Coulomb Barrier*, Daresbury, U. K., 1990, edited by M. A. Nagarajan (IOP, New York, 1991).
[31] G. Breit and M. E. Ebel, Phys. Rev. **103**, 679 (1956); **104**, 1030 (1956).
[32] K. E. Rehm, Annu. Rev. Nucl. Part. Sci. **41**, 429 (1991).
[33] J. F. Liang, L. L. Lee, Jr., J. C. Mahon, and R. J. Vojtech, Phys. Rev. C **47**, R1342 (1993).
[34] R. J. Ascuitto and E. A. Seglie, in *Treatise on Heavy-ion Science*, edited D. A. Bromley (Plenum, New York, 1984), Vol. 1, Chap. 5.